Thickness Dependence of Oxygen Reduction Reaction Kinetics on Strontium-Substituted Lanthanum Manganese Perovskite Thin-Film Microelectrodes

Citation: la O', G. J., and Y. Shao-Horn. Thickness Dependence of Oxygen Reduction Reaction Kinetics on Strontium-Substituted Lanthanum Manganese Perovskite Thin-Film Microelectrodes. Electrochemical and Solid-State Letters 12, no. 5 (2009): B82. © 2009 by ECS -- The Electrochemical Society.

As Published: http://dx.doi.org/10.1149/1.3095681

Publisher: Electrochemical Society

Persistent URL: http://hdl.handle.net/1721.1/79101

Version: Final published version: final published article, as it appeared in a journal, conference proceedings, or other formally published context

Electrochemical and Solid-State Letters, **12** (5) B82-B85 (2009)
1099-0062/2009/12(5)/B82/4/$23.00 © The Electrochemical Society

Thickness Dependence of Oxygen Reduction Reaction Kinetics on Strontium-Substituted Lanthanum Manganese Perovskite Thin-Film Microelectrodes

G. J. la O' and Y. Shao-Horn[*,z]

Electrochemical Energy Laboratory, Massachusetts Institute of Technology, Cambridge, Massachusetts 02139, USA

Oxygen reduction reaction (ORR) kinetics was investigated on dense $La_{0.8}Sr_{0.2}MnO_3$ microelectrodes as a function of temperature and microelectrode thickness using electrochemical impedance spectroscopy. The surface oxygen exchange and mixed bulk/three-phase-boundary (TPB) charge transfer process were found to control ORR kinetics at high and low temperatures, respectively. The transition temperature from the mixed bulk/TPB charge transfer control to surface oxygen exchange was found to be highly dependent on the microelectrode thickness (~600°C for 65 nm vs ~800°C for 705 nm). These findings can be used to guide the design of electrodes that can operate at intermediate temperatures.
 [DOI: 10.1149/1.3095681]

Manuscript submitted December 15, 2008; revised manuscript received February 9, 2009. Published March 12, 2009.

Solid oxide fuel cells (SOFCs) that utilize 8 mol % yttria-stabilized zirconia (YSZ) electrolyte, $La_{1-x}Sr_xMnO_3$ (LSM) cathode, and nickel-YSZ anode typically operate at temperatures above 800°C. To reduce SOFC cost and increase SOFC durability, intense research efforts have been focused on reducing operating temperatures to 700°C or lower without sacrificing SOFC efficiency.[1-3] However, the main barrier to achieve acceptable SOFC efficiency at intermediate temperatures is the voltage loss at the LSM cathode, where oxygen reduction reaction (ORR) occurs.[4] Because oxygen ion conduction is poor in LSM,[5-7] it is generally believed that the vicinity of three-phase boundaries (TPBs) of LSM cathode constitutes the active site for ORR.[8-11] Therefore, numerous studies have employed porous, high-surface-area electrodes with nanometer-scale LSM particle sizes[12-14] or composite LSM-YSZ[3,15,16] to enhance overall TPB length and thus lower ORR resistance and overpotential. However, it is not apparent how LSM particle sizes alter the rate-limiting reaction of ORR and the contributions of the TPB and bulk pathway[6,17,18] as a function of temperature, which limits the efficiency optimization of porous electrodes for intermediate temperature operation.

Electrodes with well-defined geometries, such as dense cone-shaped pellets,[19-21] thin films,[22-25] and patterned microelectrodes,[26-33] have been used to provide simple scaling relationships between ORR impedance and electrode dimensions, such as TPB length. Mizusaki et al.[6] first demonstrated that oxygen-ion diffusion can occur through dense, oxygen-over-stoichiometric LSM electrodes having thickness of 1–2 μm at 700–900°C. Brichzin et al.[28,29] have subsequently utilized microelectrodes with a thickness of 100 nm to show that ORR occurs predominantly via the bulk pathway instead of the TPB pathway at 800°C. In addition, Koep et al.[30] have used dense, patterned LSM electrodes of different thickness to show a critical thickness of 360 nm at 700°C, where the bulk pathway dominates having surface reactions as rate limiting for ORR. More recently, la O' et al.[33] have employed microelectrodes to propose four distinct processes during ORR on LSM: (*i*) ion transport in 8YSZ, (*ii*) a surface diffusion process on LSM, (*iii*) at least one surface chemical process(es) on LSM, and (*iv*) a mixed bulk/TPB charge transfer process. Our previous studies[33] suggest that the overall ORR rate can be limited by mixed bulk/TPB charge transfer processes below 700°C and surface chemical reactions above 700°C. From these studies, open questions still exist on how the critical thickness is affected by temperature and how the relative contributions of the TPB and bulk pathways to ORR are affected.

In this study, we use dense, thin-film $La_{0.8}Sr_{0.2}MnO_3$ (LSM80-20) microelectrodes to investigate the effect of different electrode thickness and temperatures on the kinetics of ORR. Using electrochemical impedance spectroscopy (EIS), we show that greater microelectrode thickness leads to increasing transition temperature, upon which surface chemical process(es), such as surface oxygen exchange, becomes the rate-limiting step for ORR relative to the bulk/TPB charge-transfer process.

Experimental

YSZ (Praxair Specialty Ceramics, USA) was initially sputtered onto alumina (Al_2O_3) substrates (MTI Crystal, USA) achieving a layer thickness of ~500 nm, which was annealed subsequently in air at 800°C for 3 h. Three LSM80-20 films of different thickness, 65, 240, and 705 nm were subsequently deposited on top of the YSZ film at 550°C. The bilayer films of LSM80-20 and YSZ supported on Al_2O_3 substrate were then annealed in air at 800°C for 10 h before any electrochemical measurements were performed. Platinum (Pt) counter electrodes were sputter-deposited adjacent to the LSM80-20 microelectrodes. Further details on the fabrication and photolithography processing are found in a previous study.[33] Microelectrode morphology was examined before and after EIS testing using optical microscopy (Mitutoyo FS-70, Kawasaki, Japan) and scanning electron microscopy [(SEM), FEI/Philips XL30 FEG ESEM, Oregon, USA].

EIS measurements of annealed LSM80-20 microelectrodes, ~190 μm in size, were performed using a microprobe station (Karl Suss, Germany) equipped with a temperature-controlled stage (Linkam TS1500, UK). EIS measurements were performed with a Solartron 1260 frequency response analyzer and a Solartron 1296 dielectric interface. EIS data were collected in the frequency range from ~1 MHz to ~ 100 μHz using an ac voltage amplitude of 10 mV and zero dc bias in the temperature range of 790–570°C in air. Microelectrode surface temperatures were confirmed using a thermocouple contacting the surface, which showed a deviation of ±5°C for each temperature set point. *ZView* software (from Scribner Associates, USA) was used to construct the equivalent circuit and perform complex least-squares fitting to deconvolute the impedance response and extract resistance and capacitance values of different processes. In the low-frequency range, two distinct semicircle arcs, labeled as LF1 and LF2, are observed. At the high-frequency region, an intercept, identified as Rs, and a linear impedance region, labeled as ALO-W, were observed. ALO-W was modeled using a finite-length Warburg element to capture the surface diffusion resistance that was hypothesized in a previous study.[33]

EIS measurements were performed using in-plane configuration, shown in the inset in Fig. 1a, which included the LSM80-20 and Pt microelectrodes side by side on the top surface of the YSZ film and spaced ~10 to 40 μm apart, as described in detail in a previous study.[33] Pt-coated tungsten carbide microneedles subsequently con-

* Electrochemical Society Active Member.
[z] E-mail: shaohorn@mit.edu

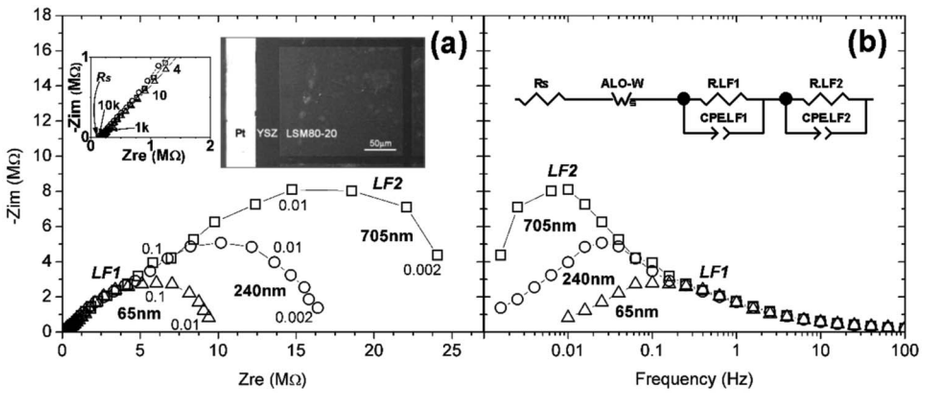

Figure 1. (a) Typical Nyquist plots from three different LSM80-20 thicknesses collected at 660°C in air showing constant LF1 while LF2 is dependent on thickness. Inset shows the high-frequency intercept Rs and a SEM image of an LSM80-20 microelectrode having thickness of 65 nm with ~190 μm size and the Pt counter electrode, which is supported on a 500 nm thick YSZ layer. All samples were tested in air at zero bias. (b) Imaginary impedance (Z_{im}) as a function of frequency showing the shift of the peak Z_{im} to lower frequencies with increased microelectrode thickness. Inset shows the equivalent circuit used to deconvolute the ORR impedance response.

tacted the LSM80-20 and Pt microelectrodes for testing. The in-plane geometry of the two-electrode LSM80-20 and Pt cell used in this study can lead to nonuniform current distributions within the electrolyte and electrode-electrolyte interface. Further experiments involving cross-plane geometries and three-electrode cells would provide further insights into the mechanism of ORR on LSM80-20.

Results and Discussion

Optical microscopy and SEM showed that LSM80-20 microelectrodes supported on YSZ after annealing were fully dense and crack free. The microelectrodes showed no significant damage after contacting with microprobe needles for EIS measurements. The sputtered LSM80-20 and YSZ films were found to be crystalline and have the rhombohedral perovskite and cubic fluorite structures after annealing, respectively.[33]

Representative complex-plane and Bode impedance plots of LSM80-20 microelectrodes with different thickness collected at 660°C in air are shown in Fig. 1a and b, respectively. All the data from LSM80-20 microelectrodes having thickness of 240 nm in this study were extracted from a previous study.[33] As expected, the high-frequency intercept attributed to ion transport in YSZ electrolyte was found to remain constant for LSM80-20 microelectrodes of different thickness, shown in the inset in Fig. 1a. Similarly, the impedance for the LF1 semicircle was found unchanged with different microelectrode thickness, as shown in Fig. 1a. As the influence of the microelectrode thickness change from 65 to 705 nm on the surface area (~40,000 μm^2) of the microelectrodes is negligible, the constant impedance response of the LF1 semicircle is in good agreement with previous findings,[33] where the LF1 process can be attributed to a surface chemical process, such as surface oxygen exchange. In contrast, the LF2 semicircle, having been attributed to mixed bulk/TPB charge transfer processes,[33] was found to have impedance dependent on microelectrode thickness, as shown in Fig. 1a. Not only did the real impedance increase, but also the peak frequency, shown in Fig. 1b, was reduced by increasing microelectrode thickness. For example, the peak frequency of the 705 nm LSM80-20 microelectrode was 1 order of magnitude lower than the microelectrode of 65 nm, as shown in Fig. 1b. These results indicate that increasing LSM80-20 electrode thickness at this temperature impedes the ORR kinetics.

The temperature dependence of the impedance of LSM80-20 microelectrodes was then examined and fitted to a standard equivalent circuit used previously,[33] as shown in the inset in Fig. 1b. The activation energy of Rs, LF1, and LF2 is shown in Fig. 2a. The activation energy of ALO-W ranged from ~1.1 to ~ 1.6 eV. As hypothesized in a previous study,[33] this suggests surface diffusion of oxygen species on LSM80-20. The Rs of microelectrodes with three different thickness was found to have comparable activation energy in the range from 1.15 ± 0.02 to 1.20 ± 0.02 eV, which falls in the upper range of activation energy of ion transport in YSZ.[34-37] The activation energy of LF1 for all microelectrodes was found to be similar in the range from 1.71 ± 0.02 to 2.02 ± 0.02 eV, which is in reasonably good agreement with previous findings on porous LSM.[11,15,25,38] The activation energy of LF2 was found to vary with microelectrode thickness, from 2.42 ± 0.02 eV for the microelectrode of 705 nm to 3.44 ± 0.03 eV for the microelectrode of

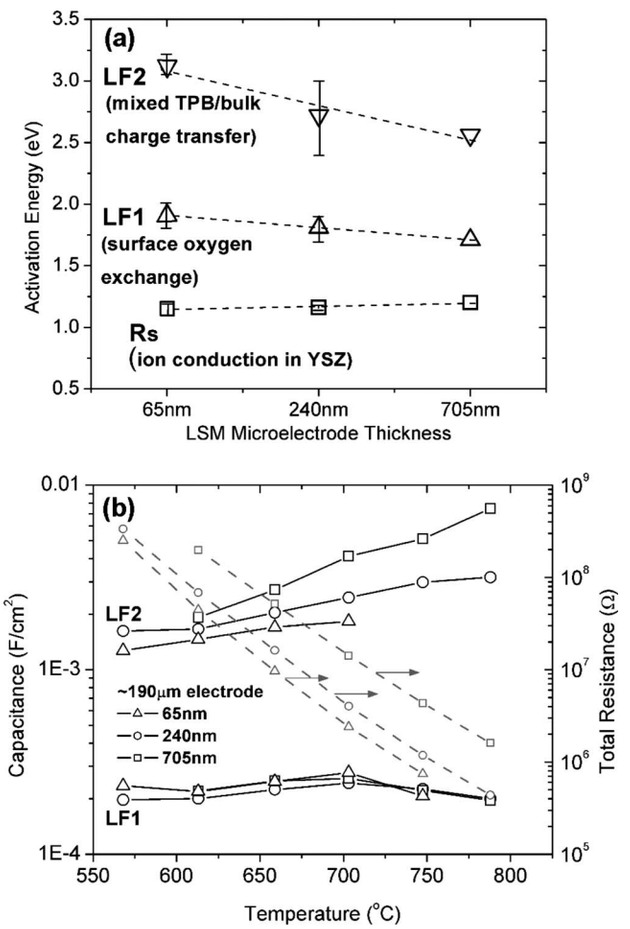

Figure 2. (a) Activation energy of ORR processes as a function of microelectrode thickness and (b) chemical capacitance as a function of temperature for LF1 and LF2 at different electrode thickness. LF1 attributed to surface oxygen exchange is observed to have fairly constant capacitance. LF2 attributed to mixed bulk/TPB process, in contrast, is observed to have a thickness-dependent capacitance due to differing microelectrode bulk volume per unit area. Total resistance for each microelectrode is plotted along the right vertical axis, showing this to decrease with higher temperature.

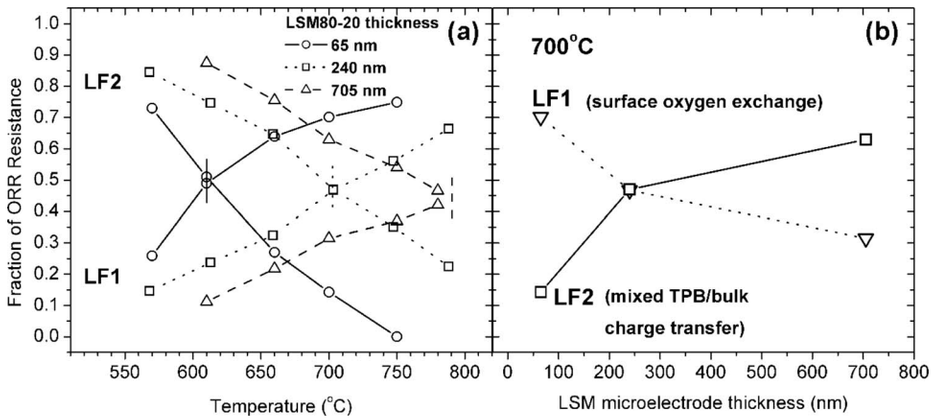

Figure 3. (a) The fraction of resistance for LF1 and LF2 in the overall oxygen reduction resistance as a function of temperature for LSM80-20 microelectrodes with thicknesses of 65, 240, and 705 nm. A shift in the transition temperature between LF1 and LF2 is observed with varying thickness. (b) The fraction of LF1 and LF2 in the overall oxygen reduction resistance as a function of microelectrode size at 700°C. Surface oxygen exchange, LF1, was found limiting for microelectrodes with thickness of <240 nm. All samples were tested in air with zero bias.

65 nm. The reported activation energy for oxygen-ion transport in LSM[7,39] is in the range of 2.6–3.0 eV. It is hypothesized that this increase in the activation energy can result from decreasing the contribution of the TPB pathway relative to the bulk pathway with decreasing the microelectrode thickness. In addition, LSM80-20 thin-film microelectrodes with nanometer-sized grains (20–70 nm), reported previously,[33] may have higher activation energy for oxygen ion diffusion, as shown by higher grain boundary activation in tracer diffusion studies than micron-sized LSM particles used in previous studies.[7,39]

As suggested by Adler,[40] chemical capacitance can provide insight into the extent of the bulk pathway contribution to ORR. Chemical capacitance of LF1 and LF2 was obtained from impedance data using the expression from Fleig,[41] $C = (R^{1-p}T)^{1/p}$, as shown in Fig. 2b. In this expression, R is the parallel resistance value in the equivalent circuit, T is the nonideal "capacitance," and p is the nonideality factor used to fit the constant phase element (CPE). T and p can be determined from the CPE expression $Z_{CPE} = 1/T(i\omega)^P$.[42] The chemical capacitance of LF1 was found to be comparable for microelectrodes of different thickness over the entire temperature range, which further supports that LF1 can be attributed to a surface chemical process, such as the surface oxygen exchange reaction on LSM80-20. For LF2, this being attributed to a mixed bulk/TPB process, the thicker electrode at higher temperatures would be expected to have a higher capacitance per unit area due to increased material. The chemical capacitance of LF2 was found to (*i*) increase with rising temperature, (*ii*) increase proportionally with the thickness at elevated temperatures where the bulk pathway was found to be more dominant (~1.2 times at 600°C to ~2.4 times at 790°C using the capacitance ratio of $LF2_{705\ nm}/LF2_{240\ nm}$), and (*iii*) have similar values for microelectrodes of different thickness at low temperatures (570°C), where the TPB pathway was dominant. These results further support the assignment of LF2 to the mixed bulk/TPB charge transfer.

To determine the rate-limiting step in ORR on LSM80-20 microelectrodes having thickness of 65, 240, and 705 nm, the ORR resistance fractions in the total impedance are plotted as a function of temperature, as shown in Fig. 3a. The ORR resistance fractions from Rs and ALO-W were each <20% of the total ORR impedance over the entire range of thickness and temperature examined. These two components did not contribute to the rate-limiting step in ORR. For the LSM80-20 microelectrode with thickness of 65 nm, the mixed TPB/bulk charge-transfer process (LF2) limits ORR at temperatures below 610°C while the surface oxygen exchange reaction (LF1) dominates the real impedance at temperatures of >610°C. The transition temperature, on which the rate-limiting process of ORR was changed from the TPB/bulk charge transfer to the surface oxygen exchange, was found to increase with greater microelectrode thickness (240 nm at ~700°C and 705 nm at ~800°C in Fig. 3a). The data in Fig. 3a is then replotted in Fig. 3b to show how the fractions of LF1 and LF2 resistance change as function of microelectrode thickness at 700°C. Because the contribution of surface oxygen exchange (LF1) to the total impedance is comparable to that of mixed TPB/bulk charge transfer (LF2) for microelectrode thickness of 240 nm, it is proposed that a LSM80-20 microelectrode with thickness of <240 nm can be considered as an effective mixed conductor. It should be mentioned that the critical thickness of 240 nm is lower than that (360 nm) reported previously by Koep et al.[30] at 700°C. This difference might be attributed to the fact that LSM80-20 microelectrodes in this work can have different microstructure and surface chemical compositions from this previous study, which could greatly affect the surface exchange and TPB/bulk charge transfer, respectively.

With decreasing temperature, the TPB pathway can become dominant for ORR on LSM80-20 as a result of increasing resistance to bulk transport of oxygen ions. In this case, LF2 impedance ratios between microelectrodes with different thicknesses should approach 1 for a given microelectrode size. At 570°C, the ratio in LF2 impedance between microelectrodes with thickness of 705 and 240 nm, $LF2_{705\ nm}/LF2_{240\ nm}$ was found to be ~1.5, which supports that the TPB pathway is dominant for ORR on LSM80-20 with thickness of >240 nm and at temperatures at <570°C. In contrast, with increasing temperature, the bulk pathway can become dominant, where the ORR impedance response should scale with electrode thickness. At 790°C, the ratio of $LF2_{705\ nm}/LF2_{240\ nm}$ impedance was found to be ~4, which is comparable to the ratio 3 of microelectrode thickness. One possible explanation for the deviation may arise from the fact the impedance values of LF1 and LF2 are comparable for the microelectrode of 705 nm at 790°C, where oxygen-ion current can have a relatively higher TPB contribution than that of the microelectrode of 240 nm. Consequently, the $LF2_{705\ nm}$ impedance is increased due to restricted bulk pathway to the overall current, which leads to the higher $LF2_{705\ nm}/LF2_{240\ nm}$ ratio than the ratio of microelectrode thickness.

Although different temperatures may induce changes in the current distributions in the in-plane configuration, it is hypothesized that these changes, if any, have no significant effect on the activation energy and transition temperature reported in this article. This hypothesis is based on the following observations: (*i*) a linear Arrhenius relationship was observed for Rs, LF1, and LF2 real resistance vs temperature on all LSM80-20 microelectrodes; (*ii*) activation energies for Rs and LF1 are found to be similar for all LSM80-20 microelectrode thicknesses tested (Fig. 2a). In addition, the activation energy values for Rs and LF1 correlate very well with the expected values for ion conduction in YSZ[34-37] and surface oxygen exchange on LSM,[11,15,25,38] respectively; (*iii*) activation energy values found for LF2 that were attributed to bulk transport in LSM in this article fall in the expected range for bulk oxygen transport in LSM.[7,39]

Insight into ORR kinetics from this microelectrode study could

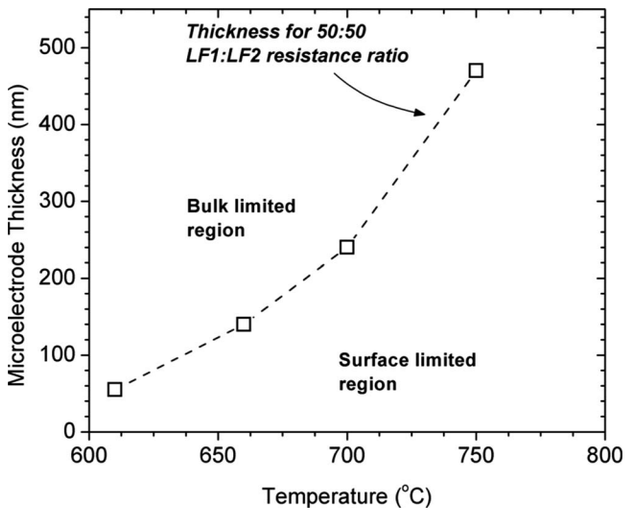

Figure 4. Transition temperature and critical thickness, where resistance from the surface oxygen exchange and mixed bulk/TPB process were found equal. Above the transition line, the LSM80-20 microelectrode is increasingly limited by bulk transport/TPB charge transfer. Below the line, surface exchange becomes rate limiting for ORR.

be potentially applied to guide the design and development of advanced LSM80-20 electrodes and micro-SOFCs that can operate at intermediate temperatures. In this study, it was found that the surface oxygen exchange could become the rate-limiting step of ORR for LSM80-20 with decreasing microelectrode thickness or at increasing operating temperature. Our results in this study allow the determination of thickness where the real impedance of the surface exchange and mixed bulk/TPB charge transfer is equal as a function of temperature, as shown in Fig. 4. Therefore, to maximize the ORR activity of LSM80-20 porous and thin-film electrodes, one would need to design microelectrode thickness or LSM80-20 particle size and choose the operating temperature to the right side of critical thickness line in Fig. 4, where the bulk pathway dominates the current for ORR. Further improvements on microelectrode performance beyond decreasing film thickness would then have to come from the enhancement of the surface exchange reaction, such as cathodic polarization treatment[43,44] and surface elemental modification.[45,46]

Conclusions

Investigation of ORR using dense, thin-film LSM80-20 microelectrodes has revealed a rate-limiting step that is dependent on operating temperature and electrode thickness. LSM80-20 thickness where the surface exchange and mixed bulk/TPB charge transfer colimit the ORR impedance is provided as a function of temperature, which can be used to serve as a guide for the design of thin-film electrodes for micro-SOFCs and porous electrodes for conventional SOFCs that can operate at temperatures lower than 700°C.

Acknowledgments

The authors thank Harry L. Tuller for fruitful discussion and helpful suggestions. This research made use of the Shared Experimental Facilities supported by the MRSEC Program of the National Science Foundation (NSF) under award no. DMR-0819762. The work was also supported, in part, by the NSF MRSEC Program under award no. DMR-0819762, and through a NSF grant no. CBET-0844526.

Massachusetts Institute of Technology assisted in meeting the publication costs of this article.

References

1. J. Fleig, *Annu. Rev. Mater. Res.*, **33**, 361 (2003).
2. S. de Souza, S. J. Visco, and L. C. De Jonghe, *J. Electrochem. Soc.*, **144**, L37 (1997).
3. A. V. Virkar, J. Chen, C. W. Tanner, and J. W. Kim, *Solid State Ionics*, **131**, 189 (2000).
4. S. C. Singhal and K. Kendall, *High Temperature Solid Oxide Fuel Cells: Fundamentals, Design, and Applications*, p. 281, Elsevier, New York (2003).
5. R. A. De Souza and J. A. Kilner, *Solid State Ionics*, **106**, 175 (1998).
6. J. Mizusaki, T. Saito, and H. Tagawa, *J. Electrochem. Soc.*, **143**, 3065 (1996).
7. I. Yasuda, K. Ogasawara, M. Hishinuma, T. Kawada, and M. Dokiya, *Solid State Ionics*, **86-8**, 1197 (1996).
8. H. Fukunaga, M. Ihara, K. Sakaki, and K. Yamada, *Solid State Ionics*, **86-8**, 1179 (1996).
9. J. Mizusaki, H. Tagawa, K. Tsuneyoshi, and A. Sawata, *J. Electrochem. Soc.*, **138**, 1867 (1991).
10. M. Mogensen and S. Skaarup, *Solid State Ionics*, **86-8**, 1151 (1996).
11. E. Siebert, A. Hammouche, and M. Kleitz, *Electrochim. Acta*, **40**, 1741 (1995).
12. K. Yamahara, C. P. Jacobson, S. J. Visco, and L. C. De Jonghe, *Solid State Ionics*, **176**, 451 (2005).
13. T. Z. Sholklapper, H. Kurokawa, C. P. Jacobson, S. J. Visco, and L. C. De Jonghe, *Nano Lett.*, **7**, 2136 (2007).
14. T. Z. Sholklapper, V. Radmilovic, C. P. Jacobson, S. J. Visco, and L. C. De Jonghe, *Electrochem. Solid-State Lett.*, **10**, B74 (2007).
15. E. P. Murray, T. Tsai, and S. A. Barnett, *Solid State Ionics*, **110**, 235 (1998).
16. M. J. L. Ostergaard, C. Clausen, C. Bagger, and M. Mogensen, *Electrochim. Acta*, **40**, 1971 (1995).
17. T. Ioroi, T. Hara, Y. Uchimoto, Z. Ogumi, and Z. Takehara, *J. Electrochem. Soc.*, **144**, 1362 (1997).
18. G. W. Coffey, L. R. Pederson, and P. C. Rieke, *J. Electrochem. Soc.*, **150**, A1139 (2003).
19. M. Odgaard and E. Skou, *Solid State Ionics*, **86-8**, 1217 (1996).
20. R. Baker, J. Guindet, and M. Kleitz, *J. Electrochem. Soc.*, **144**, 2427 (1997).
21. A. Hammouche, E. Siebert, A. Hammou, M. Kleitz, and A. Caneiro, *J. Electrochem. Soc.*, **138**, 1212 (1991).
22. A. Endo, M. Ihara, H. Komiyama, and K. Yamada, *Solid State Ionics*, **86-8**, 1191 (1996).
23. A. Endo, H. Fukunaga, C. Wen, and K. Yamada, *Solid State Ionics*, **135**, 353 (2000).
24. T. H. Ioroi, T. Y. Uchimoto, Z. Ogumi, and Z. Takehara, *J. Electrochem. Soc.*, **145**, 1999 (1998).
25. J. Van Herle, A. J. McEvoy, and K. R. Thampi, *Electrochim. Acta*, **41**, 1447 (1996).
26. T. Horita, K. Yamaji, M. Ishikawa, N. Sakai, H. Yokokawa, T. Kawada, and T. Kato, *J. Electrochem. Soc.*, **145**, 3196 (1998).
27. T. Horita, K. Yamaji, N. Sakai, Y. Xiong, T. Kato, H. Yokokawa, and T. Kawada, *J. Power Sources*, **106**, 224 (2002).
28. V. Brichzin, J. Fleig, H. U. Habermeier, and J. Maier, *Electrochem. Solid-State Lett.*, **3**, 403 (2000).
29. V. Brichzin, J. Fleig, H.-U. Habermeier, G. Cristiani, and J. Maier, *Solid State Ionics*, **152–153**, 499 (2002).
30. E. Koep, D. S. Mebane, R. Das, C. Compson, and M. Liu, *Electrochem. Solid-State Lett.*, **8**, A592 (2005).
31. E. Koep, C. Compson, M. Liu, and Z. Zhou, *Solid State Ionics*, **176**, 1 (2005).
32. R. Radhakrishnan, A. V. Virkar, and S. C. Singhal, *J. Electrochem. Soc.*, **152**, A210 (2005).
33. G. J. la O', B. Yildiz, S. McEuen, and Y. Shao-Horn, *J. Electrochem. Soc.*, **154**, B427 (2007).
34. Y. Arachi, H. Sakai, O. Yamamoto, Y. Takeda, and N. Imanishai, *Solid State Ionics*, **121**, 133 (1999).
35. S. P. S. Badwal, *Solid State Ionics*, **52**, 23 (1992).
36. J. E. Bauerle, *J. Phys. Chem. Solids*, **30**, 2657 (1969).
37. E. S. Thiele, L. S. Wang, T. O. Mason, and S. A. Barnett, *J. Vac. Sci. Technol. A*, **9**, 3054 (1991).
38. M. J. Jorgensen and M. Mogensen, *J. Electrochem. Soc.*, **148**, A433 (2001).
39. R. A. De Souza, J. A. Kilner, and J. F. Walker, *Mater. Lett.*, **43**, 43 (2000).
40. S. Adler, *Chem. Rev. (Washington, D.C.)*, **104**, 4971 (2004).
41. J. Fleig, *Solid State Ionics*, **150**, 181 (2002).
42. J. R. Macdonald, *Impedance Spectroscopy: Emphasizing Solid Materials and Systems*, p. 39, John Wiley & Sons, Hoboken, NJ (1987).
43. W. Wang and S. P. Jiang, *Solid State Ionics*, **177**, 1361 (2006).
44. S. P. Jiang, J. G. Love, J. P. Zhang, M. Hoang, Y. Ramprakash, A. E. Hughes, and S. P. S. Badwal, *Solid State Ionics*, **121**, 1 (1999).
45. Y.-K. Lee, J.-Y. Kim, Y.-K. Lee, I. Kim, H.-S. Moon, J.-W. Park, C. P. Jacobson, and S. J. Visco, *J. Power Sources*, **115**, 219 (2003).
46. A. A. Vance and S. McIntosh, *J. Electrochem. Soc.*, **155**, B1 (2008).